Pak. j. life soc. Sci. (2024), 22(1): 70-79 E-ISSN: 2221-7630;P-ISSN: 1727-4915

Pakistan Journal of Life and Social Sciences

www.pjlss.edu.pk

https://doi.org/10.57239/PJLSS-2024-22.1.006

RESEARCH ARTICLE

Multifaceted Characterization and Thermal Stability of $Y_{0.5}Sr_{0.5}Cr_{0.5}Mn_{0.5}O_3$ Chromite-Manganite Synthesized via Sol-Gel Method

Karima Seitbekova[1*], Marzhan Nurbekova[2], Mukhametkali Matayev[3], Zamira Sarsenbaeva [4], Zhadyra Durmenbayeva [5], Moldir Zhaisanbayeva[6]

[1]Abai Kazakh National Pedagogical University, Almaty, Kazakhstan

[2,3,4,5,6]Kazakh National Women's Teacher Training University, Almaty, Kazakhstan

ARTICLE INFO

Received: Sep 26, 2023

Accepted: Jan 31, 2024

Keywords

Chromite-manganite
Syngony
Sol-gel synthesis
X-ray examination
Doping
Parameters of elementary cells

***Corresponding Author:**
karimaseitbekova91@gmail.com

ABSTRACT

We studied the thermal stability and many-sided properties of $Y_{0.5}Sr_{0.5}Cr_{0.5}Mn_{0.5}O_3$ chromite-manganite that was made using the sol-gel method. We focused on the syngony type, unit cell parameters, and x-ray analysis. To confirm the results of the chromite-manganite indexing, the inverse values of the squares of interplane distances (104/d2) and the consistency of the x-ray and pycnometric densities were found to be very close to each other. It was found that the synthesised chromite-manganite crystallises in orthorhombic syngony and has a perovskite-like structure. Scanning Electron Microscopy (SEM) shows that chromite-manganite is uniformly distributed, and the crystallites are sized between 6 and 20 microns. The analysis of the relationship between heat capacity and temperature using the Thermo Gravimetry Analysis (TGA) technique demonstrates the stability of the internal structure and the presence of polymorphic transformations in the sample under study.

INTRODUCTION

Alloyed manganites of the general formula $Ln_{1-x}A_xMn_yM_{1-y}O_3$ (Ln-rare earth metal, A-alkaline earth metal, and M-transition metal) have been the subject of extensive research for use in a wide range of possible applications, such as anodes for Solid Oxide Fuel Cells (SOFC), dielectric resonators, and high-density storage devices, due to their phase diagrams as a function of chemical alloying, temperature, pressure, magnetic field, lattice mismatch, and other variables (Cowin et al., 2011; Sharma et al., 2019). There are a lot of different types of manganese perovskites. Some of the most important ones are $La_{0.5}Sr_{0.5}MnO_3$ (Maide et al., 2019; Maignan et al., 2001) and doped at A or B sites (Phan et al., 2014; Shang et al., 2015). These materials' structure and physical properties largely depend on their composition, synthesis method, and calcination temperature. Therefore, the composition and synthesis methods can regulate the properties of $La_{0.5}Sr_{0.5}MnO_3$ and related materials (Shi et al., 2010;

Shang et al., 2015; Maignan et al., 2001). Depending on the type and amount of doping, these materials exhibit various phenomena, such as charge ordering, metal-insulator transitions, multiple types of magnetic ordering, and orbital ordering in some cases. Such diverse phenomena arise as a result of the strong interaction of Mn^{3+}-O-Mn^{3+} Antiferromagnetic (AF) interactions, Mn^{3+}-O-Mn^{4+} Ferromagnetic (FM) interactions, the ordering of charges (co) Mn^{3+} и Mn^{4+} in specific cases, and Jahn-Teller distortions.

Alloying in the Mn region with other transition metals leads to a change in the Mn^{3+}/Mn^{4+} ratio, which affects the relative strength of ferromagnetic double exchange interactions against the background of a competing tendency to charge and orbital ordering of Mn^{3+} electrons. This leads to complex and incredible structural, magnetic, and electrical transport properties and opens up extraordinary opportunities for research in physics condensed matter. In this situation, the substitution of Mn ions with trivalent Cr ions provides a framework for comprehending the disorder brought about by both competing AF Mn^{4+}-O-Mn^{4+}, Cr^{3+}-O-Cr^{3+} networks and mixed Mn^{4+}-O-Cr^{3+} exchange magnetic interactions (Goveas et al., 2018; Millange et al., 2000). Alloyed manganites, characterized by the general formula Ln_1-$_x$$A_x$$Mn_y$$M_1$-$_y$$O_3$ (where Ln represents rare earth metals, A denotes alkaline earth metals, and M stands for transition metal), have emerged as prominent subjects of extensive research owing to their versatile applications. These materials exhibit diverse and tun able properties and have garnered attention for potential use in solid oxide fuel cell anodes, dielectric resonators, and high-density storage devices. Exploring their phase diagrams as functions of chemical alloying, temperature, pressure, magnetic field, and lattice mismatch has become pivotal in unraveling their multifaceted behaviours (Cowin et al., 2011; Sharma et al., 2019). Within manganese perovskites, $La_{0.5}Sr_{0.5}MnO_3$ stands out as a crucial oxide of the perovskite-type (Teng et al., 2007; Shi et al., 2010). Doping at A or B sites further enhances the adaptability of these materials (Goveas et al., 2018; Mataev et al., 2019; Phan et al., 2014; Shang et al., 2015). The manganite structure and physical properties depend on composition, synthesis method, and calcination temperature. So, $La_{0.5}Sr_{0.5}MnO_3$ and similar materials can be changed by fine-tuning the composition and changing the way they are made (Shi et al., 2010; Shang et al., 2015). This ability to change properties quickly has revealed a wide range of phenomena, such as charge ordering, metal-insulator transitions, different magnetic orderings, orbital ordering in some cases, and the appearance of Jahn-Teller distortions.

The special features of these materials come from the way Mn^{3+}-O-Mn^{3+} Antiferromagnetic (AF) and FerroMagnetic (FM) interactions work together, as well as the charge ordering of Mn^{3+}/Mn^{4+} and, in some cases, Jahn-Teller distortions (Patrin et al., 2020). The addition of other transition metals in the Mn region, known as alloying, induces a shift in the Mn^{3+}/Mn^{4+} ratio. This change affects how strong ferromagnetic double exchange interactions are compared to the Mn^{3+}electrons' tendency to charge and organize their orbitals. The outcome is a spectrum of complex and remarkable structural, magnetic, and electrical transport properties. This complexity opens up extraordinary avenues for research in condensed matter physics and materials science. To understand the disorder inherent in these alloyed manganites, replacing Mn ions with trivalent Cr ions has become a focal point of investigation. This substitution introduces a system characterized by competing antiferromagnetic networks (AF: Mn^{4+}-O-Mn^{4+}, Cr^{3+}-O-Cr^{3+}) and mixed Mn^{4+}-O-Cr^{3+} exchange magnetic interactions (Millange et al., 2000; Salje and Zhang, 2009). The complexity of the phenomena seen in alloyed manganites is already wide, but the disorder brought about by these competing networks broadens the scope of condensed matter physics research (Fonseca et al., 2008; Sirvent et al., 2022).

Research in this domain sheds light on these materials' fundamental properties and presents opportunities for technological advancements. The ability to fine-tune properties through controlled alloying and doping processes holds promise for tailoring materials to specific applications. For instance, the intricate interplay between charge ordering, metal-insulator transitions, and magnetic ordering opens avenues for developing advanced electronic and magnetic devices. The unique structural characteristics, driven by Jahn-Teller distortions and complex magnetic interactions, further contribute

to the richness of these materials' behaviours and potential applications (Martin et al., 2001; Maide et al., 2019; Yaremchenko et al., 2014). In addition, studying alloyed manganites in Solid Oxide Fuel Cells (SOFC), dielectric resonators, and high-density storage devices shows how useful they are for solving today's energy and electronics problems. The quest for materials with enhanced thermal and electrical conductivity, magnetic properties, and stability under various conditions aligns with the ever-growing demand for efficient and sustainable technologies.

In conclusion, alloyed manganites represent a captivating and promising class of materials, offering a rich tapestry of properties that can be harnessed for many applications. The ongoing study of their structural, magnetic, and electrical properties is driven by the interaction of composition, synthesis methods, and alloying strategies. This research not only adds to our basic understanding of condensed matter physics but also has the potential to change many areas of technology. As the exploration of these materials advances, the intricate dance of electrons, spins, and structures within alloyed manganites continues to unveil new frontiers in materials science and condensed matter physics.

EXPERIMENTAL

Reagents and characterization

We used "H.H." brand chromium oxide, manganese oxide, yttrium oxide, strontium carbonate, citric acid, and glycerin. Along with agate mortar, electric furnace, and muffle furnace. And distilled water to run our experiments. Furthermore, stoichiometric amounts of Y, Sr, Cr, Mn oxides, and carbonates chosen from the "H.H." brand are passed through the synthesis process. We used mechanical mixing and crushing in an agate mortar for homogeneity. Moreover, the prepared gel was heated in an electric furnace for initial solidification using an additional 2 ml of distilled water, 2 ml of glycerin, and 3 g of citric acid for gel formation. The annealing process was divided into six stages in a muffle furnace: Stage 1: 600°C, Stage 2: 700°C, Stage 3: 800°C, Stage 4: 900°C, Stage 5: 1000°C, and Stage 6: 1100°C at a temperature of 100°C/hour with a total duration of 39 hours. Moreover, intermediate grinding was performed after each annealing stage.

We applied X-ray Diffraction (XRD) to evaluate the phase composition and crystallinity after each annealing stage. Followed by the Scanning Electron Microscopy (SEM) technique to examine the surface morphology and particle size evolution. Moreover, we applied the Energy-Dispersive X-ray Spectroscopy (EDS) technique to analyze elemental composition changes further throughout the synthesis. Additionally, throughout the experiment, we assess the monophasicity and structural integrity at each synthesis stage to evaluate the impact of citric acid and glycerin on sample purity.

Formation $Y_{0.5}Sr_{0.5}Cr_{0.5}Mn_{0.5}O_3$ solid mixture

The sol-gel method was used to synthesize a solid mixture of $Y_{0.5}Sr_{0.5}Cr_{0.5}Mn_{0.5}O_3$. For this purpose, chromium oxide, manganese oxide, yttrium oxide, strontium carbonate, citric acid, and glycerin of the "H.H." brand were used as starting materials. It is shown that utilizing citric acid and glycerin as precipitators improves the monophasicity of the samples. In an agate mortar, a stoichiometric amount of oxides is mixed and crushed until a homogenous mixture is formed. To the resultant mixture, add 2 mL of distilled water, 2 mL of glycerin, and 3 g of citric acid, and then heat in an electric furnace to produce the gel. They were then exposed to repeated annealing in a muffle furnace at temperatures ranging from 600 to 1100°C, with temperature increases of 100°C every hour. Annealing was carried out in six stages. The first stage was carried out at 600°C, the second stage at 700°C, the third stage at 800°C, the fourth stage at 900°C, the fifth stage at 1000°C, and the sixth stage at 1100°C, with a total duration of 39 hours. Intermediate grinding was performed after each stage of synthesis. The groundbreaking synthesis of a solid mixture started a transformative exploration into the material world. The sol-gel method was used to make a unique composition called $Y_{0.5}Sr_{0.5}Cr_{0.5}Mn_{0.5}O_3$. A precise selection of starting materials from the "H.H." brand—chromium oxide, manganese oxide, yttrium oxide, strontium carbonate, citric acid, and glycerin—was required for the concoction. Using citric acid and glycerin as precipitators in a smart way makes this synthesis stand out, and it has a positive effect on the homogeneity of the samples that are made. The finding establishes the sol-gel process as a versatile and successful way to

create complex materials with improved structural integrity. The process begins with the precise amalgamation of stoichiometric proportions of oxides, an alchemical ballet conducted inside an agate mortar. The ensuing dance of mixing and crushing continues until homogeneity is attained, a turning point that sets the foundation for the subsequent transformative phases of the synthesis.

The intermediate grinding that serves as a pause rather than an intentional act of refining punctuates the synthesis narrative. The material is submitted to the alchemical millstone after each annealing stage, where grinding is a mechanical procedure with artisanal involvement. This meticulous step refines the material like polishing, ensuring each successive phase builds on the earlier crystalline foundations. In retrospect, this synthesis is more than just a chemical combination; it is an orchestrated symphony of materials and conditions, each of which plays an integral part in shaping the final opus. The sol-gel method appears as a maestro directing the synthesis, carefully selecting precipitators, and strategically adding water, glycerin, and citric acid. With its precise and measured temperature escalation, the annealing process is analogous to the rising crescendo in a musical masterpiece, with each stage exposing new complexities and facets of the material. A $Y_{0.5}Sr_{0.5}Cr_{0.5}Mn_{0.5}O_3$ alloy emerges from the crucible of this synthesis, not merely as a compound but as a testament to the alchemy of scientific exploration. Its structural nuances, the monophasic purity that citric acid and glycerin impart, the metamorphic heat of the electric and muffle furnaces, and the rhythmic annealing stages collectively compose a symphony, resonating with the echoes of precision and intention. This synthesis narrative extends beyond the laboratory; it encapsulates the spirit of inquiry and the quest for understanding the inherent dance of elements and conditions that shape our material world.

RESULTS AND DISCUSSION

The formation of a new phase of Chromite-Manganite was studied by x-ray phase analysis, which was performed on an x-ray diffractometer, the Miniflex 600 (Rigaku). Figure 1 presents an X-ray diffraction image of the sample. The absence of any additional reflections indicates the phase purity of the sample. The use of the sol-gel synthesis method gives the best result. Based on x-ray indexing of synthesized chromite-manganite, it was found that chromite-manganite crystallizes in the orthorhombic syngony with the following parameters of elementary cells: $Y_{0.5}Sr_{0.5}Cr_{0.5}Mn_{0.5}O_3$ – a=7.0650 Å, b=7.3750 Å, c=6.7410 Å, Z=4, $V_{el.cell}$= 342.123 Å^3, p_{x-ray} = 3.9533 g/cm^3; p_{pyc}= 3.878 g/cm^3, as given in Table 1. The average size of crystallites, as mentioned in Table 1, was calculated using the Scherrer formula as given below:

$$d = \frac{K\lambda}{\beta \cos\theta}$$

where:

d - average crystal size;

K - Scherper's constant

λ - wavelength of x-ray radiation;

β - the width of the reflex at half-height (in radians, and units of 2θ);

θ - diffraction angle (Bragg angle).

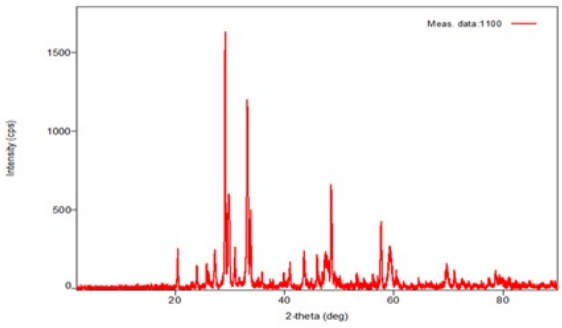

Figure 1: X-ray image of chromite-manganite composition $Y_{0.5}Sr_{0.5}Cr_{0.5}Mn_{0.5}O_3$ obtained by sol-gel method

Table 1: Type of symmetry and parameters of elementary cells $Y_{0.5}Sr_{0.5}Cr_{0.5}Mn_{0.5}O_3$

Samples	$Y_{0.5}Sr_{0.5}Cr_{0.5}Mn_{0.5}O_3$
Spatial Group	Pnma(62)
Cell Parameters (A)	
a =	7.0650 Å
b =	7.3750 Å
c =	6.7410 Å
$V_{el.cell}$ =	342.123 $Å^3$
The Average Size of Crystallites According to the Scherrer Formula	10,3 mk.
Size by SEM	11.2 mk.
p_{x-ray}	3.9533 g/cm^3
p_{pyc}	3.878 g/cm^3

The morphology and volume of chromite-manganite powder were studied by Scanning Electron Microscopy (SEM) JEOLJED-2100 with an approximation from 6 to 20 microns and the possibility of elemental analysis. The SEM images of the powder $Y_{0.5}Sr_{0.5}Cr_{0.5}Mn_{0.5}O_3$ are shown in Figure 2.

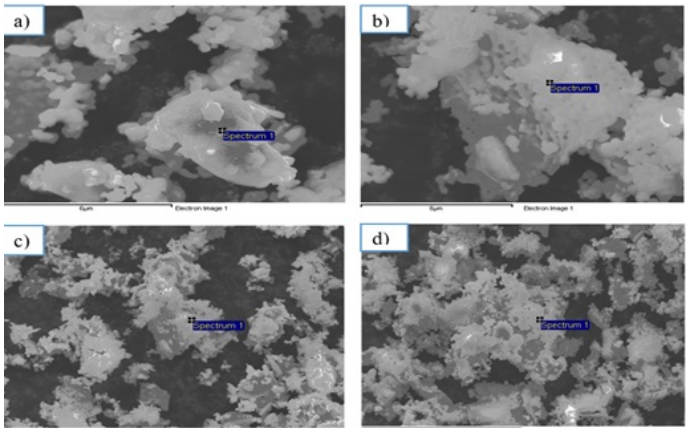

Figure 2: SEM micrographs $Y_{0.5}Sr_{0.5}Cr_{0.5}Mn_{0.5}O_3$ (a) magnification by 6 microns, (b) magnification by 6 microns, (c) magnification by 20 microns, and (d) magnification by 20 microns

Figure 2 shows the surface SEM micrographs, revealing a dense coating structure consisting of crystallites ranging in size from 6 to 20 microns. Semi-quantitative elemental analysis revealed the presence of strontium and chromium in the structure of $Y_{0.5}Sr_{0.5}Cr_{0.5}Mn_{0.5}O_3$. Elemental analysis carried out on an electron scanning microscope showed that the atomic fractions of the elements practically coincide, which corresponds to the formula of chromium and strontium-doped yttrium manganite-$Y_{0.5}Sr_{0.5}Cr_{0.5}Mn_{0.5}O_3$. The percentage ratio of chromite to manganite is presented in Table 2.

Table 2: Semi-quantitative elemental analysis of $Y_{0.5}Sr_{0.5}Cr_{0.5}Mn_{0.5}O_3$

№	Element	Weight %	Atom%
1	O K	25.26	57.47
2	Cr K	13.85	9.70
3	Mn K	12.23	8.10
4	Sr L	24.10	10.01
5	Y L	24.56	10.05
	Quantity	100.00	

The powders obtained by this technology are practically monodisperse, which is an excellent advantage of the method (Debnath et al., 2023). The data from the elemental analysis shows a good correspondence between the chemical composition and the theoretical data (Patrin et al., 2021).

The dependence of the specific heat capacity on the temperature of complex chromite-manganite was studied by differential scanning calorimutry at constant pressure in the temperature range of 57 - 1345^{o}C, as shown in Figure 3.

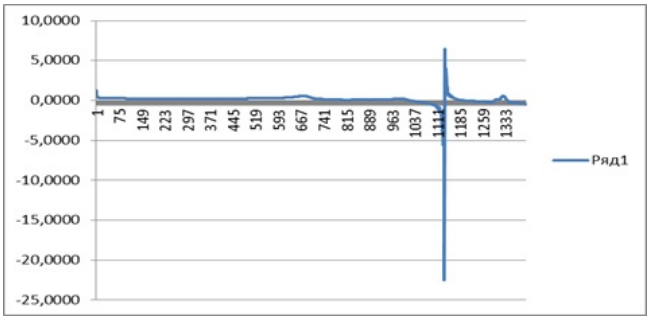

Figure 3: Dependence of specific heat capacity ranging from 57- 1345^{o}C on temperature

Table 3: Specific heat capacity data of complex chromite-manganite as a function of temperature within the temperatures of 32.37 and 1502°C

Temperature ºC	Specific Heat Capacity (J·g^{-1}·K^{-1})	Temperature ºC	Specific Heat Capacity (J·g^{-1}·K^{-1})
32,370647	1,2588	788,765503	0,2144
63,57909	0,2993	820,030823	0,1561
95,199966	0,2889	851,395325	0,1184
126,64595	0,2638	882,731811	0,0818
158,18718	0,2431	914,377747	0,0933
189,663818	0,2254	946,129395	0,0950
221,183914	0,2215	977,979492	0,0999
252,345017	0,2105	1009,875122	0,1033
284,000977	0,2109	1041,543701	0,1533
316,023865	0,2184	1073,34021	0,2482
347,856873	0,2271	1116,79834	-0,0615
380,097809	0,2222	1117,832642	-0,0532
412,268219	0,2237	1118,928223	-0,0696
444,353027	0,2233	1200,409546	-0,8148
476,201508	0,2302	1232,088013	1,1752
507,947357	0,2383	1263,61145	0,1841
539,607117	0,2499	1295,136841	-0,0093
570,973938	0,2778	1326,509888	-0,0868
602,511597	0,2837	1358,037353	-0,1583
633,586975	0,2968	1389,682373	-0,1843
664,774536	0,3285	1421,158936	0,4629
695,718201	0,3959	1452,79895	-0,2630
726,693665	0,5232	1484,308228	-0,3597
757,863403	0,4676	1502,02832	-0,4676

The results show that in this temperature range, there is a jump at a temperature of 1117^{o}C, which proves the stability of the internal structure and the absence of polymorphic transformations in the sample under study. As a result of magnetostatic measurements, it was found that hysteresis magnetization loops

are observed at low temperatures. Below 30^{o}C, the hysteresis loop is open, but the magnetization saturation is not achieved up to the field H = 50 kOe. At temperatures T > 35^{o}C, the magnetization curve is hysteresis-free and is typical for a paramagnet, with the straight line slope significantly dependent on the measurement temperature, as shown in Figure 4.

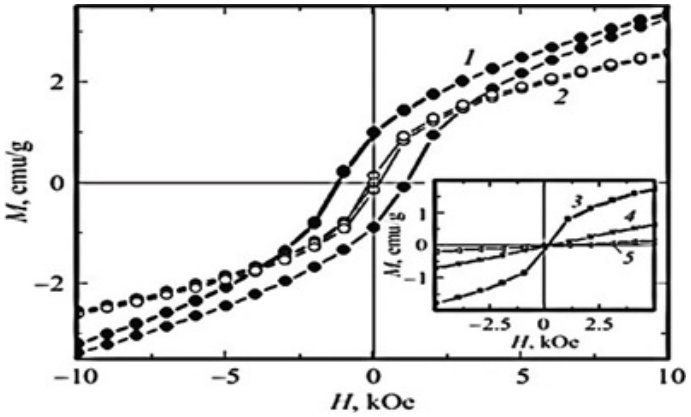

Figure 4: Field dependence of polycrystal magnetization $Y_{0.5}Sr_{0.5}Cr_{0.5}Mn_{0.5}O_3$. Curves 1, 2, 3, 4, 5 for T = 4.5, 25, 35, 75, 170^{o}C, respectively.

When the $Y_{0.5}Sr_{0.5}Cr_{0.5}Mn_{0.5}O_3$ (polycrystal magnetization) is heated, two different types of temperature magnetization curves are produced. These depend on the background: either cooling in a magnetic field (FC) or cooling in a field with no magnetic field (ZFC). Just at a temperature of T ≈ 35^{o}C in the ZFC mode, a maximum occurs in small magnetic fields depending on polycrystal magnetization $Y_{0,5}Sr_{0,5}Cr_{0,5}Mn_{0,5}O_3$. In fields of about 2.5 kOe, a low-temperature "tail" of magnetization appears, the specific gravity of which increases with an increase in the measurement field. In higher fields of measurement, the maximum is smoothed, and in fields H > 40 kOe, it practically does not appear, as shown in Figure 5.

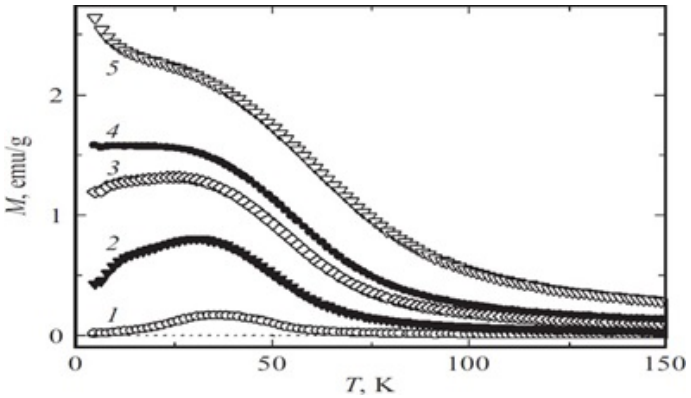

Figure 5: Temperature dependences of polycrystal magnetization $Y_{0.5}Sr_{0.5}Cr_{0.5}Mn_{0.5}O_3$. Curves 1, 2, 3, 4, 5 for H = 0.15, 1.0, 2.5, 3.5, 7.5 kOe, respectively.

Figure 6 shows temperature dependences of the inverse susceptibility (1/χ) obtained in different magnetic fields (for a standard two-sublattice antiferromagnet (Patrin et al., 2020) $\chi = C/(T - 2)$, where C is a constant, T is the temperature, and 2^{o}C is the intersection point of the asymptote

with the abscissa axis, depending on the ratio of intra- and inter-lattice exchanges). The insert shows how 1/χ changes for an antiferromagnet when the magnetic field moves in different directions along the axis of antiferromagnetism. It can be seen that the experimental dependence of 1/χ(T) qualitatively matches the antiferromagnetic ordering for a polycrystal (Troyanchuk et al., 2006). For the measurement field H = 2.5 kOe, the bend on the curve 1 /χ(T) begins to manifest itself clearly in the region TN ≈ 75–90 K, which can be associated with the temperature of the Neel. For all measurement fields, the value 2 is -27^{o}C, whereas the temperature TN depends on the measurement field. For monocrystalline manganites, as a rule, the inter-lattice interaction is noticeably greater within the sublattice interaction. In our case, the average size of the crystallites is quite important (≈ 10.3 mkm). Furthermore, along with the magnetic order inside the crystallites, there is an intercrystalline exchange interaction, which can have a comparable magnitude with the exchange inside the crystallites. Then, there is a competition of interactions. The presence of a low-temperature magnetization tail in large magnetic fields indicates the presence of a superparamagnetic subsystem, and, as shown in Mataev et al. (2020), the behaviour in weak magnetic fields for the La–Sr–Mn-Cr system (with a low Cr content) is similar to spin-glass. This gives reason to believe that the granules are ferromagnetic and randomly oriented in space, and antiferromagnetic interaction takes place between the granules. At the same time, intercrystalline exchange interactions should be less than intracrystalline.

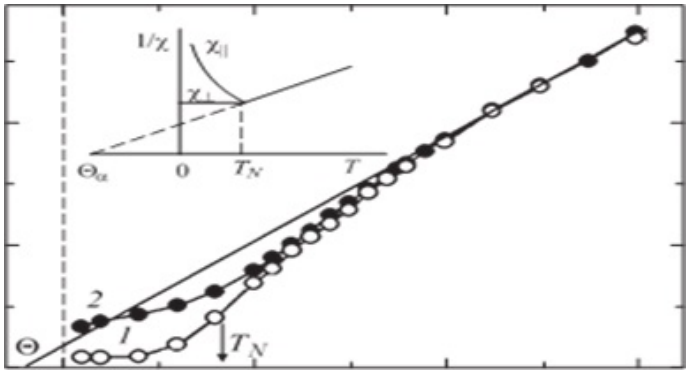

Figure 6: Temperature dependences of the reverse susceptibility. 1 - 2.5 kOe, 2 - 40 kOe. In the insert, the model dependence for 1/χ(T) is taken from (Taran et al., 2015)

CONCLUSION

This study used the sol-gel method to successfully make a new solid solution of chromite-manganite with the formula $Y_{0.5}Sr_{0.5}Cr_{0.5}Mn_{0.5}O_3$. Some of the things that were looked into were the x-ray, psychometric, and synonym types of the newly formed chromite-manganite. The indexing results of chromite-manganite were supported by the fact that the calculated and experimental values of the inverse squares of interplane distances (104/d2) and the densities measured by x-ray and pycnometry were the same. The findings revealed that the synthesized chromite-manganite adopts an orthorhombic syngony and features a perovskite-like structure. The SEM analysis showed that the chromite-manganite has a single-distribution structure, with crystallite sizes ranging from 6 to 20 microns. Using the TGA method to study how heat capacity changes with temperature gave us useful information about how stable the structure was inside the sample and whether any polymorphic changes were happening. The results presented herein contribute significantly to understanding the structural and thermal properties of the $Y_{0.5}Sr_{0.5}Cr_{0.5}Mn_{0.5}O_3$ chromite-manganite. The fact that the crystallites are all the same size and have an orthorhombic syngony, along with the fact that the structure is similar to a perovskite, shows how precise the sol-gel method is.

Moreover, the TGA results underscore the stability of

the internal structure, establishing the groundwork for potential applications in various fields. This study expands the knowledge base surrounding alloyed manganites, specifically those containing yttrium, strontium, chromium, and manganese, and opens avenues for further exploration into their potential applications. The careful use of citric acid and glycerin as precipitators and the controlled annealing process show a careful way to make monophasic samples. This sets a standard for future research in perovskite-type oxides. In conclusion, this study not only gives a thorough look at the synthesized manganite-chromite, but it also adds to our knowledge of alloyed manganites and the many uses they can have. The meticulous synthesis process, coupled with comprehensive characterization techniques, positions this work as a significant step forward in the exploration of perovskite-type oxides, paving the way for future advancements in materials science and condensed matter physics.

ACKNOWLEDGEMENT

Abai University (Kazakhstan) has funded, was funding, or is funding this research (Contract No. 09-02-55/261 dated March 28, 2023).

REFERENCES

Cowin PI, Petit CT, Lan R, Irvine JT, Tao S; 2011. Recent progress in the development of anode materials for solid oxide fuel cells. Advanced Energy Materials, 1(3):314-332.

Debnath M, Bose E, Pal S; 2023. Impact of non-magnetic Zn^2+ doping on the structural, magnetic and magnetocaloric properties of $Nd_{0.5}Ca_{0.5}Mn_{1-x}Zn_xO_3$ (x= 0, 0.05, 0.10) compounds. Journal of Magnetism and Magnetic Materials, 575:170752.

Fonseca F, Muccillo E, Muccillo R, De Florio D; 2008. Synthesis and electrical characterization of the ceramic anode La_{1-x} Sr $_x$ $Mn_{0.5}Cr_{0.5}O_3$. Journal of the Electrochemical Society, 155(5):B483.

Goveas LR, Bhat S, et al.; 2018. Occurrence of Mixed Phase in Bi0. $5Sr_{0.5}Mn_{0.9}Cr_{0.1}O_3$ bulk sample: Electron Paramagnetic Resonance and Magnetization Studies. Applied Magnetic Resonance, 50 (9):1049-1058.

Maide M, Paiste P, Möller P, Lust E, Nurk G; 2019. Influence of A-and B-Site modifications of ($La_{1-x}Sr_x$) $yCr_{0.5}$-$zMn_{0.5}$-wNiz+ wO_3-δ on electrochemical impedance characteristics of reversible solid oxide cell. Journal of The Electrochemical Society, 166(15):F1148.

Maignan A, Martin C, Hervieu M, Raveau B; 2001. Ferromagnetism and metallicity in the $CaMn_{1-x}Ru_xO_3$ perovskites: A highly inhomogeneous system. Solid State Communications, 117(6):377-382.

Martin C, Maignan A, Hervieu M, Autret C, Raveau B, Khomskii D; 2001. Magnetic phase diagram of Ru-doped Sm $_{1-x}$ Ca $_x$ MnO_3 manganites: Expansion of ferromagnetism and metallicity. Physical Review B, 63(17):174402.

Mataev M, Patrin G, Seitbekova KZ, Tursinova ZY, Abdraimova M; 2019. Synthesis and x-ray diffraction study of the chromite-manganites $Y_(1 - X)MeCr_{0,5}Mn_{0,5}O_3$ (Me = Mg, Ba, Sr, x≈0,7). Chemical Journal of Kazakhstan, p. 207-216.

Mataev M, Patrin G, Seitbekova K, Tursinova Z; 2020. Synthesis and magnetic properties of $Y_{0.5}Ca_{0.5}Cr_{0.5}Mn_{0.5}O_3$ compounds. Bulletin of the Eurasian National University named after LN Gumilyov. Series: Chemistry. Geography. Ecology, 133(4):35-43.

Millange F, De Brion S, Chouteau G; 2000. Charge, orbital, and magnetic order in $Nd_{0.5}Ca_{0.5}MnO_3$. Physical Review B, 62(9):5619.

Patrin GS, Mataev MM, Seitbekova KZ, Shiyan YG, Yarikov SA, Zharkov SM; 2020. Magnetic and resonance properties of the $Y_{0.5}Sr_{0.5}Cr_{0.5}Mn_{0.5}O_3$ polycrystal. Physics of the Solid State, 62:1350-1354.

Patrin G, Mataev M, Seitbekova KZ, Shiyan YG, Plekhanov V; 2021. Magnetic and resonance properties of the $Y_{0.5}Sr_{0.5}Cr_{0.5}Mn_{0.5}O_3$ polycrystal. 2103(1):012199.

Phan TL, Thanh T, Yu S; 2014. Influence of co doping on the critical behavior of $La_{0.7}Sr_{0.3}Mn_{1-x}Co_xO_3$. Journal of Alloys and Compounds, 615:S247-S251.

Salje E, Zhang H; 2009. Domain boundary engineering. Phase Transitions, 82(6):452-469.

Shang C, Xia Z, Wei M, Chen B, Jin Z, Huang J, et al.; 2015. Dynamical behavior of step-like transition of $La_{0.5}Sr_{0.5}Mn_{1-x}TixO_3$ in a widened field sweep rate. Ceramics International, 41(8):9708-9714.

Sharma H, Kumar D, Tulapurkar A, Tomy C; 2019. Effect of B-site bismuth doping on magnetic and transport properties of $La_{0.5}Ca_{0.5}Mn_{1-x}$ B_i x O_3 thin films. Journal of Materials Science, 54(1):130-138.

Shi L, Yang H, Zhou S, Zhao J, He L, Zhao S, et al.; 2010. Influence of annealing atmosphere on the properties of $Y_{0.5}Sr_{0.5}Cr_{0.5}Mn_{0.5}O_3$. Solid State Communications, 150(7-8):371-374.

Sirvent JdD, Carmona A, Rapenne L, Chiabrera F, Morata A, Burriel M, et al.; 2022. Nanostructured $La_{0.75}Sr_{0.25}Cr_{0.5}Mn_{0.5}O_3$–Ce0. 8Sm0. 2O2 Heterointerfaces as All-Ceramic Functional Layers for Solid Oxide Fuel Cell Applications. ACS Applied Materials & Interfaces, 14(37):42178-42187.

Taran S, Sun C, Huang C, Yang H, Nigam A, Chaudhuri B, et al.; 2015. Electrical and magnetic properties of Y-doped $Y_{0.5}Sr_{0.5}Cr_{0.5}Mn_{0.5}O_3$ manganite system: Observation of step-like magnetization. Journal of Alloys and Compounds, 644:363-370.

Teng F, Han W, Liang S, Gaugeu B, Zong R, Zhu Y; 2007. Catalytic behavior of hydrothermally synthesized $La_{0.5}Sr_{0.5}MnO_3$ single-crystal cubes in the oxidation of CO and CH4. Journal of Catalysis, 250(1):1-11.

Troyanchuk I, Bushinsky M, Karpinsky D; 2006. Magnetic ordering in manganites substituted by chromium ions. Journal of Experimental and Theoretical Physics, 103:580-588.

Yaremchenko A, Kharton V, Kolotygin V, Patrakeev M, Tsipis E, Waerenborgh J; 2014. Mixed conductivity, thermochemical expansion and electrochemical activity of Fe-substituted (La, Sr)(Cr, Mg) O_3- δ for solid oxide fuel cell anodes. Journal of Power Sources, 249:483-496.